Nanoscale

Characterization and Manipulation of Single Nanoparticles Using Nanopore-Based Electrokinetic Tweezer

Journal:	*Nanoscale*
Manuscript ID	NR-ART-10-2019-008476
Article Type:	Paper
Date Submitted by the Author:	02-Oct-2019
Complete List of Authors:	Yazbeck, Rami; Boston University Alibakhshi, Mohammad; Boston University Von Schoppe, Joseph; Boston University Ekinci, Kamil; Boston University Duan, Chuanhua; Boston University

Nanoscale

Paper

Characterization and Manipulation of Single Nanoparticles Using Nanopore-Based Electrokinetic Tweezer

Rami Yazbeck, Mohammad Amin Alibakhshi, Joseph Von Schoppe, Kamil L. Ekinci and Chuanhua Duan*

Received,
Accepted,
DOI: 10.1039/x0xx00000x

Rsc.li/nanoscale

Manipulation and characterization of nanoscale objects through electrokinetic techniques offer numerous advantages compared to existing optical methods and hold great potential for both fundamental research and practical applications. Here we present a novel electrokinetic tweezer for single nanoparticle manipulation and characterization based on electrokinetic trapping near a low-aspect-ratio nanopore. We find that this nanopore-based electrokinetic tweezer share lots of similarity with optical tweezers and can be modeled as an overdamped harmonic oscillator, with the spring constant of the system being the trap stiffness. We show that different values of ionic currents through the nanopore and trap stiffnesses are achieved when trapping nanoparticles with different sizes (down to 100 nm) and/or zeta potentials. We also demonstrate that the trap stiffness and nanoparticle position can be easily tuned by changing the applied voltage and buffer concentration. We envision that further development of this electrokinetic tweezer will enable various advanced tools for nanophotonics, drug delivery, and biosensing.

1. Introduction

Nanoscale objects such as viruses, bacteria, and engineered nanoparticles are involved in numerous biological, chemical and physical processes.[1-3] Developing techniques that can manipulate and characterize individual nanoscale objects in solutions are thus of paramount importance for a broad spectrum of applications ranging from medical diagnostics and homeland security to photonics and nanoelectronics.[1, 4-7]

To date, optical techniques such as optical tweezers and optical resonators are the most notable methods for manipulating/ characterizing single nanoscale objects. These techniques rely on optical gradient forces to achieve trapping and manipulation of nanoscale objects and use trapping-induced changes of optical properties (e.g. resonant frequency, transmitted laser intensity) to achieve detection and characterization[8-13]. While the optical approaches are well established and have been extensively used in basic biophysics research and biosensing, the cost of the laser and the bulky optical elements limit their applications in lab-on-a-chip devices.[14] Furthermore, since the optical gradient force and the changes of optical properties scale with the volume of the object, it is still challenging to use the optical techniques to manipulate and characterize small nanoscale objects.[15, 16]

Because of these limitations, development of facile non-optical methods for manipulating and characterizing nanoscale objects that scale more favorably with object size is highly desired. One of the promising direction is electrokinetic techniques as they have fewer equipment requirements and are more suitable for characterizing and manipulating nanoscale objects.[17-20]

In fact, various nano/microfluidic-based resistive pulse sensing techniques have been developed for the detection and characterization of nanoscale objects.[21-23] These techniques use changes of ionic current/resistance (and the corresponding noise and time duration) associated with translocation of nanoscale objects through micro/nanoscale conduits to achieve detection and characterization, showing the capability of detecting even single biomolecules (~nm in size).[24-27] On the other hand, a few electrokinetics-based single nanoparticle trapping and manipulation methods have also been reported. Chad *et al*. used drag forces produced by electroosmotic flow to control the movement of single quantum dots with a size of 6 nm.[28] Ndukaife *et al*. demonstrated trapping of polystyrene nanoparticles with a diameter of 300 nm using a new trapping paradigm based on electrothermoplasmonic flow.[29]

Despite these successes, electrokinetic techniques that can simultaneously achieve nanoparticle characterization and manipulation have yet to be developed. Here we report a tunable electrokinetic tweezer for precise nanoparticle characterization/ manipulation. This electrokinetic tweezer is based on electrokinetic trapping of nanoparticles near nanopores.[30, 31] We, however, for the first time discover that such electrokinetic trapping displays similar dynamics to that of an optical tweezer and can be modeled as an

Department of Mechanical Engineering, Boston University, Boston, Massachusetts, 02215, USA. E-mail: duan@bu.edu

† Electronic Supplementary Information (ESI) available. See DOI: 10.1039/x0xx00000x

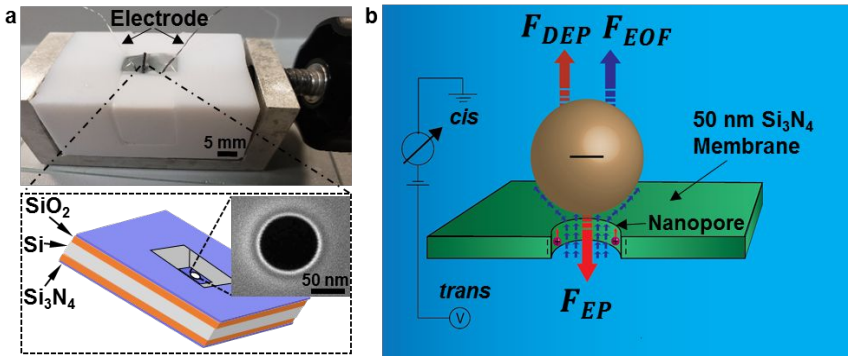

Fig. 1 Nanopore-based electrokinetic trapping setup and trapping mechanism. (a) Experimental setup showing our nanopore device separating two reservoirs each with an electrode and a schematic diagram of the nanopore device. Inset: an SEM image of the nanopore milled with FIB. (b) Schematic illustration showing the working principle of electrokinetic trapping of a single nanoparticle near a low aspect ratio nanopore.

overdamped harmonic oscillator driven by random thermal fluctuations. We investigate how the trap stiffness (i.e. the spring constant of the harmonic oscillator) and the trapping-induced change of ionic current through the nanopore are affected by the size and zeta potential of the trapped nanoparticle and show that they can be simultaneously used for nanoparticle characterization, making this electrokinetic tweezer a powerful characterization tool. We also find that the nanoparticle trapping location and the spring constant of the harmonic oscillator can be easily tuned by changing the applied voltage and/or buffer concentration. Consequently, the nanopore-based electrokinetic tweezer also has great potential for nanoparticle manipulation.

Fig. 1a shows our nanopore setup, which consists of two reservoirs connected only by a low-aspect-ratio silicon nitride nanopore (pore thickness is smaller than the pore diameter). Each reservoir is filled with an aqueous solution and equipped with silver/silver chloride (Ag/AgCl) electrodes connected through an ammeter and voltage source. In this study, we used silicon nitride (Si_3N_4) nanopores that are 50 nm in thickness and 90 nm in diameter. When an external electric field is applied across the pore a steady current can be measured. Our approach for trapping nanoparticles is achieved by intentionally designing the diameter of the nanopore to be smaller than that of the particles of interest. When a charged nanoparticle is introduced into one of the reservoirs, due to the applied bias it will experience an electrophoretic force (F_{EP}) and migrate toward the pore. In the meantime, if the nanopore has the same type of surface charges as the nanoparticle, an electroosmotic flow in the opposite direction of nanoparticle migration will be generated, exerting a drag force (F_{EOF}) on the nanoparticle. While these two forces cannot totally counterbalance with each other due to the same dependence on the local electric field ($F_{EP/EOF} \propto E$), there is an additional dielectrophoretic force (F_{DEP}) acting on the nanoparticle due to the non-uniform DC electric field. This dielectrophoretic force points towards the lowest electric field ($F_{DEP} \propto \nabla E^2$) and thus tends to push the nanoparticle away from the nanopore. Because of the different dependence on the electric field, the interplay of these three forces would lead to a force balance position near the nanopore, which causes trapping of the nanoparticle and a decrease of translocation ionic current (Fig. 1b).[32]

The particle will stay in the trap as long as the external voltage is applied. Moreover, since the trapped nanoparticle is not physically in contact with the nanopore, the particle can easily be released from the pore by simply inverting the electric field polarity, setting back the current to the open state again.

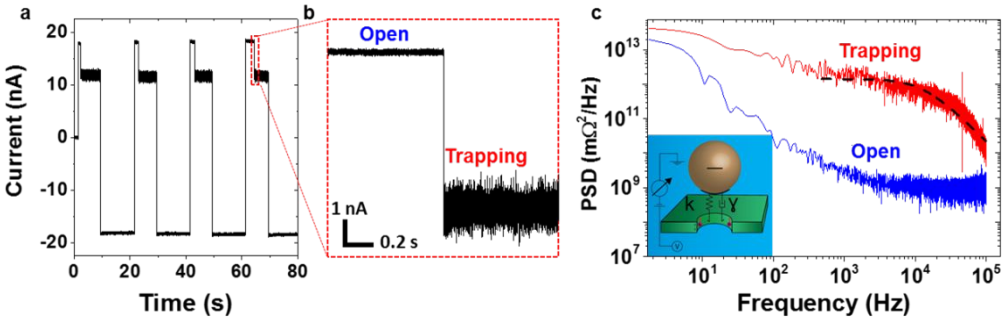

Fig. 2 Experimental results of trapping/releasing 100 nm PS-COOH nanoparticles. (a) Typical time trace of an ionic current signal of repeated trapping and release of 100 nm PS-COOH beads through a 90-nm silicon nitride nanopore at 200 mV (see supplementary Information S1 for extended ionic trace). (b) A zoom-in on a single trapping event showing the ionic current before trapping (open state) and in the trapped state. (c) Power spectral density (PSD) of the resistance fluctuations with respect to frequency (double-logarithmic axes) in two different cases: trapped and open state. The dashed line represents the best fit line of the theoretical model to the experimental trapped signal. Inset: schematic illustration of a trapped particle near a nanopore as a harmonic oscillator. *K* represents the stiffness of the spring and γ is the friction coefficient of the damper.

2. Results and discussion

2.1. Evaluation of the signal of a trapped nanoparticle

Fig. 2a shows typical current trace displaying multiple trapping and releasing events under a capture voltage of +0.2 V pulse and a release voltage of -0.2 V pulse (both durations are 10 s) for 100-nm diameter carboxylated polystyrene (PS-COOH) nanoparticles. When first applying the positive bias, the nanopore is open and the current is measured to be 18 nA. After applying the positive bias for a short period, a trapping event occurs, which is shown as a decrease in the current from 18 nA to 12 nA. When the voltage is reversed, the current becomes -18 nA, which suggests that trapping is no longer taking place and the nanopore reopen instantly. The nanoparticle has been instantly released from the trap.

We found that such trapping-induced current blockage did not change for over a two hundred trapping/releasing cycles (Fig. S2). The blockage current is also not a function of nanoparticle concentration (Fig. S3). Furthermore, variation of the current blockage only depends on the types of nanoparticles in solution, i.e., solutions with only one type of nanoparticles would only show one type of blockage current and solutions with two types of nanoparticles would show two types of blockage currents that match the blockage currents measured from two solutions each with one type of nanoparticles, respectively (Fig. S4). These results confirm that the observed trapping phenomenon under our experimental conditions is always caused by single nanoparticles which is similar to what have been reported by Tsutsui *et al*.[30] and Lee *et. al*.,[33] but different from the observation of multiple-particle electrokinetic trapping near the tip of a glass nanopipette.[32]

Beside the trapping-induced current change, we have noticed that there is a significant increase in the noise level of the current when a particle is trapped (Fig. 2b). Such an increase of noise was not observed in previous experiments, probably due to the low sensitivity of their instrument (they used a low-pass filter with 10 kHz cut-off frequency).[30, 31] The increased noise is unlikely a result of electroosmotic-flow-induced hydrodynamic vortices at the pore entrance. While the electroosmotic flows around the negatively charged mobile nanoparticle and the negatively charged fixed nanopore are opposite in direction and may result in hydrodynamic vortices, we were not able to observe such vortices using fluorescent nanoparticles. Furthermore, we also have tried nanopore blockage using positively charged nanoparticles (see supplementary information S3). In such cases, the nanoparticles would not be trapped near the nanopore, but physically block the pore due to strong electrostatic interactions with the pore surface. We found that the corresponding blockage currents were larger than those in the trapping cases and after blockage the positively charged nanoparticles could not be released using reverse bias. As the particle surface and pore surface have opposite charges, electroosmotic flows from those two immobile nanostructures should also be in opposite directions, which would lead to the formation of hydrodynamic vortices and noise increase. However, we found that the current noise did not increase for such nanopore blockage events (Fig. S5).

We believe that the increased noise in our trapping experiment is actually a sign of Brownian motion of the nanoparticle,[34] which means that the trapped particle is not immobilized but is instead vibrating around the trapping position and therefore can be modelled as a harmonic oscillator driven by random thermal fluctuations (Fig. 2b).[35, 36] Consequently, this electrokinetic trap can be used as an electrokinetic tweezer, sharing similar functions with an optical tweezer yet with a potentially better control and sensitivity for nanoparticles.

As the characteristics of the harmonic oscillator can also provide information about the nanoparticle, which have been widely demonstrated in optical tweezers, we analyse the current noise by looking at the power spectral density (PSD) (see supplementary Information S4). The PSD quantifies the noise power present in the signal as a function of frequency per unit frequency; this the commonly used method to study optically trapped beads.[35, 37, 38] Fig. 2b shows the measured resistance PSD with respect to frequency in two different cases: trapped and open state (i.e. in the absence of trapped particle). The PSD curve for the trapped case is three orders of magnitude higher than that for the open-state case and shows several interesting characteristics. The PSD first decreases with the increasing frequency at low frequency (below 0.5 kHz) and then shows a plateau at intermediate frequencies (approximately from 0.5 kHz to 10 kHz) before decreasing at higher frequencies again. While the first descending curve is clearly 1/f noise in the measurement,[39] the plateau and the second descending curve are the spectral characteristics of a damped harmonic oscillator. Moreover, since there is no resonant frequency near the corner frequency (turnover point), this harmonic oscillator is actually overdamped and the effect of inertia is negligible.[38]

The PSD of an overdamped harmonic oscillator can be modelled by a Lorentzian:[38, 40]

$$PSD(f) = \frac{2}{\pi} * \frac{\gamma * k_B T * \beta^2}{K^2 + \gamma^2 * w^2} \quad (1)$$

where, $k_B T$ represents the thermal energy; K is the spring constant, which is a measure of the trapping strength. β is the linear transduction sensitivity of the system in units of Ω/m, which relates the change in resistance to the displacement of the particle. w is the radial frequency; $w = 2\pi f$, f is the temporal frequency. The drag coefficient γ can be approximated from Stokes' law for a spherical particle: $\gamma = 3\pi\eta d$, where d is the particle diameter and η is the dynamic viscosity of bulk water. We fitted Equation (1) to the experimental PSD from 0.5 kHz to 1000 kHz in order extract both K and β for the trapped nanoparticles at a specific voltage.

2.2. Dependence of trapping-induced normalized current change and trap stiffness on nanoparticle size and surface charge

We performed the trapping experiment and current (noise) analysis using nanoparticles with different sizes and/or surface charge densities (see tabulated results and PSD figures respectively in the supplementary Information S5 and S6) and studied the dependence of current change and spring constant on nanoparticle size and surface charge density for nanopores with an aspect ratio of 056 (see discussion on the effect of aspect ratio in the supplementary Information S7). For each nanoparticle type, a 150 pM concentration of the nanobeads suspended in 1x PBS solution was

used. All nanoparticles used in this study were bought from Bangs Laboratories, Inc. Before the trapping experiments, we analysed the size distribution as well as the zeta potential of each of the different nanoparticle solutions in 1x PBS using dynamic light scattering (DLS, Brookhaven 90 Plus Nanoparticle Sizer).

To study the size effect, we tested 100, 155 and 350 nm polystyrene nanoparticles modified with carboxyl group. DLS measurements have showed that these nanoparticles have a narrow size distribution and similar zeta potentials. Fig. 3a shows the normalized current change ($\Delta I = (I_{open} - I_{Trapped})/I_{open}$) for the different nanoparticles under different capture voltage. The results indicate that, giving the same applied voltage, the normalized current change increases with the increasing nanoparticle size. This is relatively easy to understand, as a large nanoparticle will prevent more ions from entering the pore and thus increases the entrance resistance. In contrast with the increasing current change, the spring constant extracted from the noise analysis showed an inverse dependence on the nanoparticle size. As shown in Fig. 3b, the spring constant actually decreases with the increasing nanoparticle size. Since the spring constant in this case is the slope of the net electrokinetic force–nanoparticle position curve near the equilibrium position and the net electrokinetic force should be closely related to the intensity of the local electric field, which would decrease when farther away from the nanopore,[41] this different dependence indicates that the equilibrium position of the larger nanoparticles is farther away from the nanopore.

We also studied the effect of surface charge density on the trapping current change and spring constant of the electrokinetic tweezer. For this study, carboxyl-functionalized and amine-functionalized polystyrene nanoparticles were tested. Both of the two nanoparticles have a mean diameter of 100 nm with small size distribution. However, the carboxyl functionalized polystyrene nanoparticles (PS-COOH) have a zeta potential of -32 mV ± 2 mV while the amine functionalized polystyrene (PS-NH_2) have a zeta potential of -10 mV ± 2 mV. Fig. 3c shows the results obtained for a capture voltage of 200 mV for both particle types.

Our results show that the PS-COOH nanoparticles cause higher current change than their PS-NH_2 counterparts during trapping. This means that the carboxyl particles are able to exclude more ions from entering the pore. Given that both nanoparticles have the same size, the only explanation for this difference is that the PS-COOH beads get trapped at an equilibrium position much closer to the pore than the PS-NH_2 particles. This closer equilibrium position can be explained as a result of the higher surface charge density of the PS-COOH nanoparticles, which resulted in a higher electrophoretic force in those nanoparticles for the same location. Consequently, in the equilibrium position for PS-NH_2 nanoparticles, PS-COOH particles still experience a net pushing force and thus will be pushed closer to a new position that is closer to the nanopore where the electroosmotic flow induced force increases and can re-balance the electrophoretic force.

This explanation is also supported by the extracted spring constants. As listed in Fig. 3c, PS-COOH nanoparticles show higher spring constants compared with their PS-NH_2 counterparts. When the nanoparticle equilibrium position is closer to the nanopore, the corresponding electric field intensity becomes larger and the net electrokinetic force exerted on the nanoparticle become larger when the nanoparticle is away from the equilibrium position, leading to larger spring constants and more stable trapping.

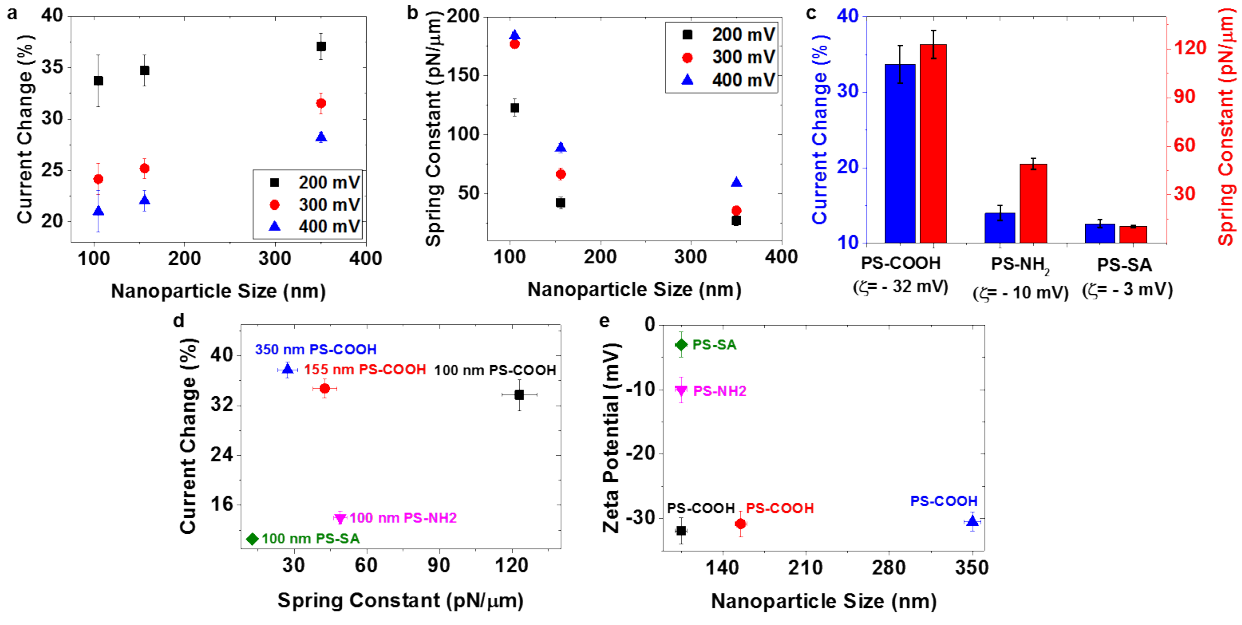

Fig. 3 Experimental results of nanoparticles with different sizes and/or surface charges trapped near a 90 nm pore. (a) Normalized current change between the open and trapped state current and (b) spring constant of the 100, 155 and 350 nm PS-COOH particles at different applied voltages. (c) Normalized current change and spring constant from the trapped signal of 100 nm PS-COOH and 100 nm PS-NH_2 at 200 mV. (d) ΔI V.S. K for the five tested nanoparticles at 200 mV. (e) Mean diameter and zeta potential of all the nanoparticles used for this study as obtained with DLS.

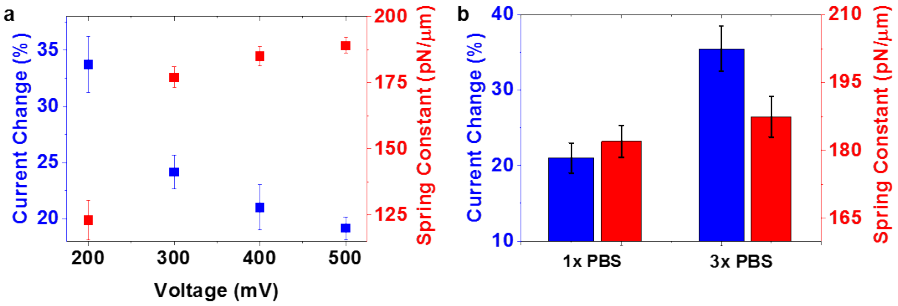

Fig. 4 Experimental results on 100 nm PS-COOH particles using 90 nm SiN nanopore. (a) Normalized current change between the open and trapped state current and spring constant of 100 nm PS-COOH particles suspended in 1x PBS buffer at different applied voltages. (b) Normalized current change and spring constant from the trapped signal of 100 nm PS-COOH in 1x and 3x PBS at 400 mV.

We would like to add that, using the mechanism shown in Fig. 1a, we can only trap and characterize nanoparticles with zeta potentials (surface charge densities) higher than the nanopore otherwise the nanoparticles cannot be captured by the nanopore – the electroosmotic drag force will be always larger than electrophoretic force.[41] However, it is still possible to use this electrokinetic tweezer to trap and characterize nanoparticles with zeta potentials (and surface charge densities) lower than the nanopore but with the same sign (see discussion on nanopore blockage by particles with opposite surface charges in supplementary information S3). In such a case, a reverse bias is used and the electroosmotic driving force becomes the force that drives the nanoparticles towards the nanopore. We demonstrated this alternative electrokinetic trapping using streptavidin functionalized polystyrene (PS-SA) nanoparticles with a mean diameter of 100 nm and a zeta potential of -3 mV ± 2 mV. The PS-Streptavidin nanoparticles showed a mean normalized current change of 12.6% and mean spring constant of 10.6 pN/μm, both of which are smaller than the PS-NH_2 nanoparticles, indicating that the equilibrium position for the PS-SA nanoparticles is farther away from the nanopore.

Nevertheless, it is clear from the above studies that both the normalized current change and the spring constant strongly depend on the size and surface charge density of the nanoparticles. However, it is important to mention that the corresponding dependence is significantly different. Consequently, we can build a 2-D ΔI (normalized ionic current) V.S K (spring stiffness) index to characterize and differentiate different nanoparticles. Fig. 3d and 3e plots the corresponding locations of the five tested nanoparticles in the ΔI V.S. K and size V.S. zeta potential (surface charge density) respectively. In both figures, each nanoparticle corresponds to a unique location. Consequently, this electrokinetic tweezer is better than existing single nanoparticle characterization techniques, which usually can only detect and differentiate the nanoparticle by a single index, either their size,[42] surface charge density[43] or size to surface charge density ratio.[44]

2.3. Dependence of trapping-induced normalized current change and trap stiffness on applied voltage and buffer concentration

In addition to harnessing this electrokinetic tweezer for nanoparticle detection and characterization, we also explore its potential for nanoparticle manipulation, including changing the nanoparticle position and the trap stiffness. For this goal, we have studied the effect of applied voltage and buffer concentration on the electrokinetic trapping because these two parameters are the only two that we can tune for a given nanopore and a target nanoparticle. For this study, we have used the same 90 nm nanopore, and the 100 nm PS-COOH nanoparticles suspended in 1x PBS. Fig. 4a plot the current change and the spring constant as a function of applied voltage. The normalized current change decreases with the increasing voltage (Fig. 4a). Given that the normalized current change is essentially the normalized conductance change and the open-state conductance of this system remains unchanged for all applied voltage, it is straightforward to tell that the nanoparticle equilibrium positions changes with the applied voltage, becoming farther away from the nanopore as the applied voltage increases. However, this does not mean that the trapping becomes less stable. In fact, the trap stiffness (the spring constant) still increases with the increasing applied voltage (Fig. 4a). We believe that the increasing trap stiffness results from the overall increase of the electric field. Nevertheless, the change of equilibrium position is not expected and rather counter-intuitive as one would expect at a larger applied voltage, the nanoparticle would experience larger electrophoretic force and thus get pushed closer to the nanopore. We hypothesize that these unexpected results stem from voltage-caused concentration polarization near the nanoparticle despite the relatively high salt concentration of the buffer solution. Such polarization would change the local ionic concentration and lead to a decrease in the electric field in front of the nanoparticle.[45-47] Since higher voltage would cause more concentration polarization, the decrease of the local electrical field may be higher than the overall increase of the electric field due to the increasing voltage, causing nanoparticles being pushed further away from the nanopore.

To verify this hypothesis and also study the effect of buffer salt concentration, we tested trapping the same PS-COOH nanoparticles at 1x and 3x PBS buffer solutions using the same applied bias; the results are plotted in Fig. 4b. We indeed observed that high concentration solutions leads to more current change and larger spring constant. Similar to our previous discussion, these results suggest that the nanoparticle equilibrium position is closer to the nanopore in more concentrated buffer solution. Since higher concentration in general cause less polarization because of more ions and smaller Debye screening length,[48] these results do not only

demonstrate that polarization could affect the electrokinetic trapping, but also show that we can manipulate nanoparticle trapping position along the axis of the nanopore by simply tuning the buffer concentration.

3. Conclusions

This work describes a novel nanopore-based electrokinetic tweezer for trapping, manipulating and characterizing nanoparticles with single-nanoparticle resolution and high-sensitivity. This technique has shared ground with both resistive pulse and optical sensing giving it an advantage over existing characterization methods. We experimentally demonstrated the applicability and feasibility of this electrokinetic tweezer by studying the dependence of trapping-induced normalized current change and trap stiffness on nanoparticle size, surface charge, voltage, and buffer concentration. Our results show that all these factors can significantly affect the trapping properties. The former two can be used for nanoparticle detection and characterization and the latter two can be used for nanoparticle manipulation. This nanopore-based electrokinetic tweezer thus holds great promise for developing new techniques for applications in biosensing, nanophotonics, nanopore gating as well as in fundamental biophysics research.

4. Experimental Section

4.1 Nanopore device fabrication

The bulk of our nanopore device consists of a <100> silicon substrate that has an approximate thickness of 500 μm. As the first step, a 2 μm insulating layer of silicon dioxide (SiO_2) film was grown on both sides of the silicon by wet thermal oxidation. The SiO_2 layer reduces the capacitive noise in the measured signal of these devices. A 50 nm nitride is then deposited on top of the SiO_2 layer using low-pressure chemical vapor deposition (LPCVD) to create a low-stress, amorphous silicon nitride (Si_3N_4) layer. Through standard photolithographic and etching techniques, a free-standing silicon nitride membrane with an area of roughly of 20 μm x 20 μm is created. A nanopore is then drilled through the membrane using a highly focused gallium ion beam (FEI Quanta 3D FEG FIB) operating at 30 kV.

4.2 Experimental Setup

Prior to testing, the nanopore devices were cleaned in a piranha solution (96% sulfuric acid/ 30% hydrogen peroxide, 3:1) at 120 °C for 10 minutes, then thoroughly rinsed by a stream of deionized water and dried gently with nitrogen. The nanopore surface can be further treated with oxygen plasma to make the wetting process easier. The chip surface around the membrane was painted with a fast cure silicone rubber adhesive (Sil-Poxy). This was found to further reduce the capacitance noise during the measurement. The chips were then loaded into a custom piranha-resistant Teflon holder and sealed with silicone adhesive to separate cis and *trans* chambers. The only connection between the two chambers is the nanopore itself. Both reservoirs are filled with an electrolyte buffer. Our experimenters were performed with a 1x phosphate-buffered saline (PBS, Sigma Aldrich) equivalent to 150 mM NaCl at pH 7.4 (unless otherwise noted).

An electric potential in voltage-clamp mode was sourced across the nanopore through silver/silver chloride (Ag/AgCl) electrodes. The resulting ionic current was monitored with an amplifier (Axon 200B, Molecular Devices, Inc). The output current was digitized at a sampling rate of 500 kHz (Digidata 1550 digitizer, Molecular Devices, Inc.) and conditioned by an eight-pole low-pass filter with a 100 kHz cut-off frequency. The setup was placed in a Faraday cage on a floating air table to minimize any external electromagnetic radiation and the vibrational interference. The RMS noise of the devices was in the range of 300 pA.

4.3 Electrical measurements

An electric potential in voltage-clamp mode was sourced across the nanopore through silver/silver chloride (Ag/AgCl) electrodes. The resulting ionic current was monitored with an amplifier (Axon 200B, Molecular Devices, Inc). The output current was digitized at a sampling rate of 500 kHz (Digidata 1550 digitizer, Molecular Devices, Inc.) and conditioned by an eight-pole low-pass filter with a 100 kHz cut-off frequency. The setup was placed in a Faraday cage on a floating air table to minimize any external electromagnetic radiation and the vibrational interference. The RMS noise of the devices was in the range of 300 pA.

The first step in each experiment was to measure the conductance of the nanopore device and check how it compares to the theoretical model. This step was to confirm the dimensions of the nanopore and to make sure that the pore is neither blocked nor damaged. The device was tested only if the difference between the experimental and theoretical conductance was lower than 10%. Then nanoparticles were placed in the *cis* chamber, which is grounded. Upon applying a bias in the *trans* chamber the particle is electrophoretically driven toward the nanopore. The trapping events were then observed in the form of a drop in the ionic current and in an increase in the noise power. Such data recording were then extracted and analysed with Patch-Clamp software (Molecular Devices, Inc.).

Conflicts of interest

Authors do not have any conflict of interest.

Acknowledgements

We thank the Photonics Center at Boston University for the use of their fabrication and characterization facilities. We acknowledge the contributions of R. Agen for his assistance in the noise analyses. In addition, we acknowledge several other lab-mates in the Nanoscale Energy-Fluids Transport Laboratory at Boston University, including S. Xiao, Y. Xu, and H. Chen for their great help on this work. The work was supported by the DARPA Young Faculty Award Program (No. D18AP00048).

References

1. A. Kaur and U. Gupta, *J. Mater. Chem.*, 2009, **19**, 8279-8289.
2. N. F. Steinmetz, *Nanomedicine*, 2010, **6**, 634-641.
3. E. C. Wang and A. Z. Wang, *Integr. Biol.*, 2014, **6**, 9-26.
4. S. K. Bose, C. P. Lawrence, Z. Liu, K. S. Makarenko, R. M. J. van Damme, H. J. Broersma and W. G. van der Wiel, *Nature Nanotechnology*, 2015, **10**, 1048-1052.
5. I. Gehrke, A. Geiser and A. Somborn-Schulz, *Nanotechnology Science and Applications*, 2015, **8**, 1-17.
6. G. R. Rudramurthy and M. K. Swamy, *J Biol Inorg Chem*, 2018, 1185–1204.
7. P. K. Jain, K. S. Lee, I. H. El-Sayed and M. A. El-Sayed, *J Phys Chem B*, 2006, **110**, 7238-7248.
8. A. Ashkin, J. M. Dziedzic and T. Yamane, *Nature*, 1987, **330**, 769-771.
9. K. Dholakia, P. Reece and M. Gu, *Chem. Soc. Rev.*, 2008, **37**, 42-55.
10. A. Jesacher, S. Furhapter, S. Bernet and M. Ritsch-Marte, *Opt. Express.*, 2004, **12**, 4129-4135.
11. Y.-F. Chen, X. Serey, R. Sarkar, P. Chen and D. Erickson, *Nano Lett.*, 2012, **12**, 1633-1637.
12. S. Mandal, X. Serey and D. Erickson, *Nano Lett.*, 2010, **10**, 99-104.
13. M. Baaske and F. Vollmer, *Chemphyschem*, 2012, **13**, 427-436.
14. R. Quidant and C. Girard, *Laser Photonics Rev.*, 2008, **2**, 47-57.
15. J. P. Gordon, *Phys. Rev. A.*, 1973, **8**, 14-21.
16. O. M. Marago, P. H. Jones, P. G. Gucciardi, G. Volpe and A. C. Ferrari, *Nat. Nanotechnol.*, 2013, **8**, 807-819.
17. S. Prakash, M. Pinti and B. Bhushan, *Philos. Trans. R Soc. A*, 2012, **370**, 2269-2303.
18. R. Karnik, R. Fan, M. Yue, D. Li, P. Yang and A. Majumdar, *Nano Lett.*, 2005, **5**, 943-948.
19. C. Dekker, *Nat. Nanotechnol.*, 2007, **2**, 209-215.
20. H.-C. Chang and L. Y. Yeo, *Electrokinetically driven microfluidics and nanofluidics*, Cambridge Univ. Press, Cambridge, 1st ed. edn., 2010.
21. W. Zhao, B. Wang and W. Wang, *Lab Chip*, 2016, **16**, 2050-2058.
22. M. Wanunu, *Phys. Life Rev.*, 2012, **9**, 125-158.
23. C. Duan, M. A. Alibakhshi, D.-K. Kim, C. M. Brown, C. S. Craik and A. Majumdar, *ACS NANO*, 2016, **10**, 7476-7484.
24. J. J. Kasianowicz, E. Brandin, D. Branton and D. W. Deamer, *Proc. Natl. Acad. Sci. U.S.A.*, 1996, **93**, 13770-13773.
25. H. Bayley and C. R. Martin, *Chem. Rev.*, 2000, **100**, 2575-2594.
26. M. A. Alibakhshi, J. R. Halman, J. Wilson, A. Aksimentiev, K. A. Afonin and M. Wanunu, *ACS NANO*, 2017, **11**, 9701-9710.
27. V. Kara, C. Duan, K. Gupta, S. Kurosawa, D. J. Stearns-Kurosawa and K. L. Ekinci, *Lab Chip*, 2018, **18**, 743-753.
28. C. Ropp, R. Probst, Z. Cummins, R. Kumar, A. J. Berglund, S. R. Raghavan, E. Waks and B. Shapiro, *Nano Lett.*, 2010, **10**, 2525-2530.
29. J. C. Ndukaife, Y. Xuan, A. G. A. Nnanna, A. V. Kildishev, V. M. Shalaev, S. T. Wereley and A. Boltasseva, *ACS NANO*, 2018, **12**, 5376-5384.
30. M. Tsutsui, Y. Maeda, Y. H. He, S. Hongo, S. Ryuzaki, S. Kawano, T. Kawai and M. Taniguchi, *Applied Physics Letters*, 2013, **103**, 013108.
31. A. Arima, M. Tsutsui, Y. H. He, S. Ryuzaki and M. Taniguchi, *Aip Advances*, 2016, **6**, 115004.
32. L. Shi, A. Rana and L. Esfandiari, *Scientific reports*, 2018, **8**, 6751.
33. S. Lee, Y. H. Zhang, H. S. White, C. C. Harrell and C. R. Martin, *Anal Chem*, 2004, **76**, 6108-6115.
34. F. Gittes and C. F. Schmidt, *European Biophysics Journal with Biophysics Letters*, 1998, **27**, 75-81.
35. Y. Deng, J. Bechhoefer and N. R. Forde, *Journal of Optics a-Pure and Applied Optics*, 2007, **9**, S256-S263.
36. R. M. Simmons, J. T. Finer, S. Chu and J. A. Spudich, *Biophysical Journal*, 1996, **70**, 1813-1822.
37. K. Berg-Sorensen, E. J. G. Peterman, T. Weber, C. F. Schmidt and H. Flyvbjerg, *Review of Scientific Instruments*, 2006, **77**, 063106.
38. K. Berg-Sorensen and H. Flyvbjerg, *Review of Scientific Instruments*, 2004, **75**, 594-612.
39. R. M. Smeets, U. F. Keyser, N. H. Dekker and C. Dekker, *Proc Natl Acad Sci U S A*, 2008, **105**, 417-421.
40. Y. Pang, H. Song, J. H. Kim, X. Hou and W. Cheng, *Nat Nanotechnol*, 2014, **9**, 624-630.
41. M. Davenport, K. Healy, M. Pevarnik, N. Teslich, S. Cabrini, A. P. Morrison, Z. S. Siwy and S. E. Letant, *Acs Nano*, 2012, **6**, 8366-8380.
42. W. J. Lan, D. A. Holden, B. Zhang and H. S. White, *Anal. Chem.*, 2011, **83**, 3840-3847.
43. M. Firnkes, D. Pedone, J. Knezevic, M. Doblinger and U. Rant, *Nano Lett.*, 2010, **10**, 2162-2167.
44. R. Vogel, A. K. Pal, S. Jambhrunkar, P. Patel, S. S. Thakur, E. Reategui, H. S. Parekh, P. Saa, A. Stassinopoulos and M. F. Broom, *Scientific reports*, 2017, **7**, 17479.
45. A. Mani, T. A. Zangle and J. G. Santiago, *Langmuir*, 2009, **25**, 3898-3908.
46. S. Das, P. Dubsky, A. van den Berg and J. C. T. Eijkel, *Physical Review Letters*, 2012, **108**, 138101.
47. S. Marczak, K. Richards, Z. Ramshani, E. Smith, S. Senapati, R. Hill, D. B. Go and H. C. Chang, *Electrophoresis*, 2018, 2029 -2038.
48. L. H. Yeh, K. L. Liu and J. P. Hsu, *Journal of Physical Chemistry C*, 2012, **116**, 367-373.

Table of Content

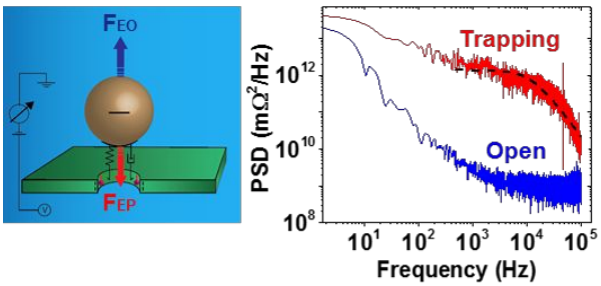

We developed a nanopore-based DC electrokinetic tweezer and demonstrated its great potential for single nanoparticle characterization and manipulation.